CHEMISTRY
A EUROPEAN JOURNAL

Supporting Information

Structure and Dynamics of Triazole-Linked DNA: Biocompatibility Explained

André Dallmann,*[a, b] Afaf H. El-Sagheer,[c, d] Lars Dehmel,[a] Clemens Mügge,[a] Christian Griesinger,[e] Nikolaus P. Ernsting,[a] and Tom Brown*[c]

chem_201102979_sm_miscellaneous_information.pdf

1 DNA synthesis

General method for oligonucleotide synthesis and purification

Standard DNA phosphoramidites, solid supports, and additional reagents were purchased from Link Technologies, Applied Biosystems and Proligo. Oligonucleotides were synthesized on an Applied Biosystems 394 automated DNA/RNA synthesizer or AKTAOligopilot Plus synthesizer using a standard 1.0 or 15.0 μmol phosphoramidite cycle of acid-catalyzed detritylation, coupling, capping, and iodine oxidation. Stepwise coupling efficiencies and overall yields were determined by the automated trityl cation conductivity monitoring facility and in all cases were $> 98.0\,\%$. All β-cyanoethyl phosphoramidite monomers were dissolved in anhydrous acetonitrile to a concentration of 0.1 M immediately prior to use. The coupling time for the 3'-propargyl dT (T^K) and 5'-iodo dT phosphoramidite monomers was changed from the standard 40 s to 480 s.

The unmodified oligonucleotides were purified by reversed-phase HPLC on a Gilson system using PLRPS column (Varian) with a gradient of acetonitrile in ammonium acetate (0 % to 50 % buffer B over 30 min, flow rate 4 mL/min), buffer A: 0.1 M ammonium acetate, pH 7.0, buffer B: 0.1 M ammonium acetate, pH 7.0, with 50 % acetonitrile. Elution was monitored by UV absorption at 300 nm. After HPLC purification, oligonucleotides were desalted on an ACTA purifier using a Hiprep 26/10 desalting column and analyzed by gel electrophoresis.

i) Synthesis of the 3'-alkyne oligonucleotide (ODN-1) (5'-fragment)

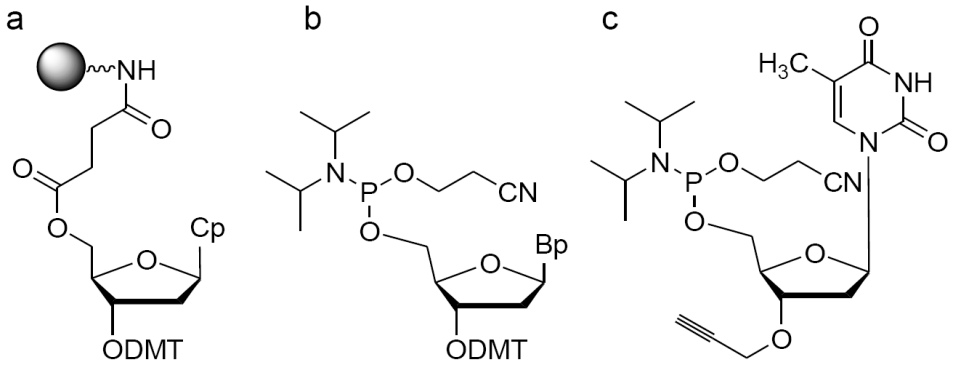

Fig. S1: *Assembly of 3'-alkyne dT oligonucleotide. Use reverse support (a) and phosphoramidites (b) and add 3'-propargyl dT (c) as final addition.*

3'-Alkyne oligonucleotide was synthesized (12 X 1.0 μmol synthesis) using the 3'-propargylthymidine phosphoramidite monomer and assembling the required sequence in the 5'- to 3'-direction using the 3'-O-(4,4'-dimethoxytrityl) deoxyribonucleoside-5'-phosphoramidites of A, G, C and T (reverse phosphoramidites, Link Technologies). The oligonucleotide was then cleaved and deprotected by exposure to concentrated aqueous ammonia for 60 min at room temperature followed by heating in a sealed tube for 5 h at 55 °C. The ammonia was removed by evaporation and the oligonucleotide was dissolved in water then extracted with dichloromethane to remove the protecting groups. It was then used for the click reaction without further purification.

ii) Synthesis of the 5'-azide oligonucleotide (ODN-2) (3'-fragment)

The oligonucleotide was assembled on the 15.0 μmol scale (trityl-off) as described in the general method above using the commercially available 5'-iodo dT monomer (Glen Research). To convert the 5'-iodo dT to 5'-azido dT, sodium azide (50 mg) was suspended in dry DMF (1 mL), heated for 10 min at 70 °C then cooled down and the supernatant taken up into a 1 mL syringe, passed back and forth through the column then left at room temperature overnight. Another fresh solution of sodium azide was then made and it was passed back and forth through the column and left at room temperature for another 4 h. The column was then washed with DMF and acetonitrile and dried by passing a stream of argon gas through it. The resultant 5'-azide oligonucleotide was cleaved from the solid support and deprotected by heating the column (filled with concentrated aqueous ammonia solution) in an oven for 6 h at

55 °C. The column was cooled down then washed three times with 50 % ethanol in water. The three washes were collected, evaporated then redissolved in water and extracted with dichloromethane to remove the protecting groups. The oligonucleotide was used in the click reaction without further purification.

iii) Synthesis of the unmodified oligonucleotides

The unmodified oligonucleotides were synthesised on 1.0 or 15.0 μmol scale. For the 1.0 μmol scale, cleavage from the solid support and deprotection were performed as described above for the alkyne oligonucleotide. For the 15.0 μmol scale, cleavage from the solid support and deprotection were performed as described above for the azide oligonucleotide.

Code	Oligonucleotide sequences 5'-3'	Calc. mass	Found mass
ODN-1	CGACGT^{K}	1831	1831
ODN-2	^{Z}TTGCAGC	2121	2122
ODN-3	FTTTTTTTTTTGCTGCAAACGTCG	nd	nd
ODN-4	CGACGTtTTGCAGC	3952	3952
ODN-5	GCTGCAAACGTCG	3960	3959
ODN-6	CGACGTTTGCAGC	nd	nd

^{z} = 5'-azide, ^{k} = 3'-propargyl, t = -triazole linkage, F = fluorescein, nd=not done.
Mass spectra were recorded on a Bruker micrOTOF™ II focus ESI-TOF MS instrument in ES^{-} mode.

Fig. S2: *Oligonucleotide Sequences and mass spectrometry results.*

iv) Synthesis of the 13-merTAL oligonucleotide (ODN-4)

Alkyne (ODN-1), azide (ODN-2) and splint (ODN-3) oligonucleotides (8.0 μmol of each) in 0.2 M NaCl (2.0 mL) were annealed by heating at 95 °C for 5 min, cooled down slowly to room temperature then kept at 4 °C for 1 h. A solution of CuI click catalyst was prepared from tris-hydroxypropyltriazole ligand (0.28 mmol in 0.2 M NaCl, 300.0 μL), sodium ascorbate (0.4 mmol in 0.2 M NaCl, 100.0 μL) and $CuSO_4 \cdot 5\,H_2O$ (0.04 mmol in 0.2 M NaCl, 100.0 μL). This solution was added to the annealed oligonucleotides and the reaction mixture was kept at 4 °C for 1 h, then kept at room temperature for another 1 h. Reagents were removed using a NAP-25 gel-filtration column. The ligated oligonucleotide was purified by anion-exchange HPLC on a Gilson HPLC system using a Resource Q anion-exchange column (6 mL volume, GE Healthcare). The following protocol was used: run time 16 mins, flow rate 5 mL per min, binary system, gradient: time in mins (% buffer B); 0 (0); 3 (0); 4 (40); 9.5 (80); 10 (100); 12 (100); 13 (0); 15.5 (0); 16 (0). Elution buffer A: 0.01 M aqueous NaOH, 0.05 M aqueous NaCl, pH 12.0, buffer B: 0.01 M aqueous NaOH, 1 M aqueous NaCl pH 12.0. Elution of oligonucleotide was monitored by ultraviolet absorption at 295 nm. After FPLC purification the oligonucleotide was desalted using NAP-25 then NAP-10 Sephadex gel-filtration columns (GE Healthcare), analysed by gel electrophoresis and characterized by mass spectrometry.

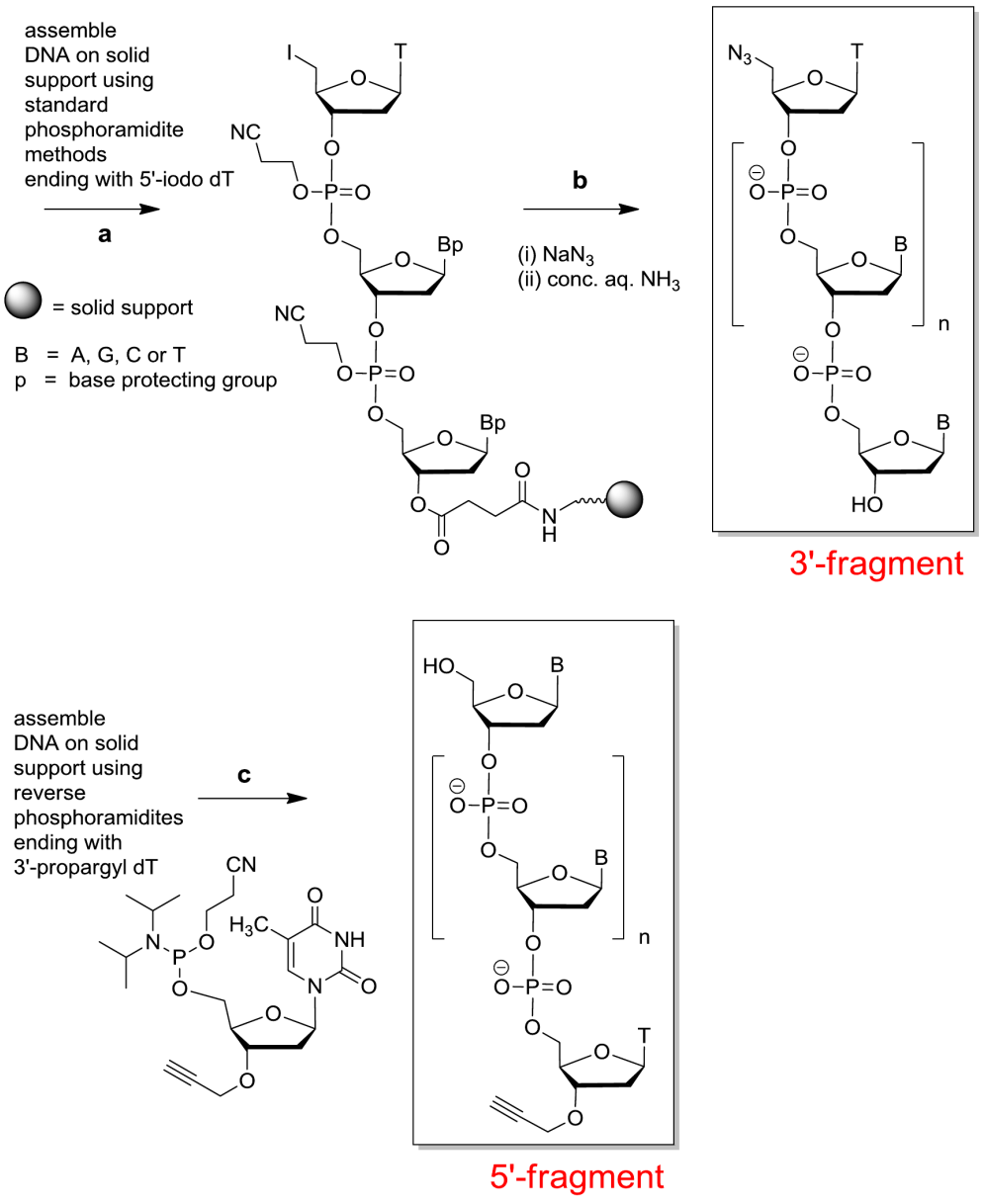

Fig. S3: *Synthesis of the 3'-alkyne oligonucleotide, 5'-azide oligonucleotide and click ligaterd 13-mer TAL*

2 UV Melting analysis

UV melting was monitored by optical absorption at 260 nm using a Varian Cary 4000 Scan UV-Visible Spectrophotometer. The solutions had a total duplex concentration of 3 μM, with 10 mM phosphate buffer, 200 mM NaCl at pH 7.0 The optical path length was 1 cm, the temperature was varied between 20 and 85 °C at 1 °C/min. T_m values were calculated using Cary Win UV Thermal application Software.

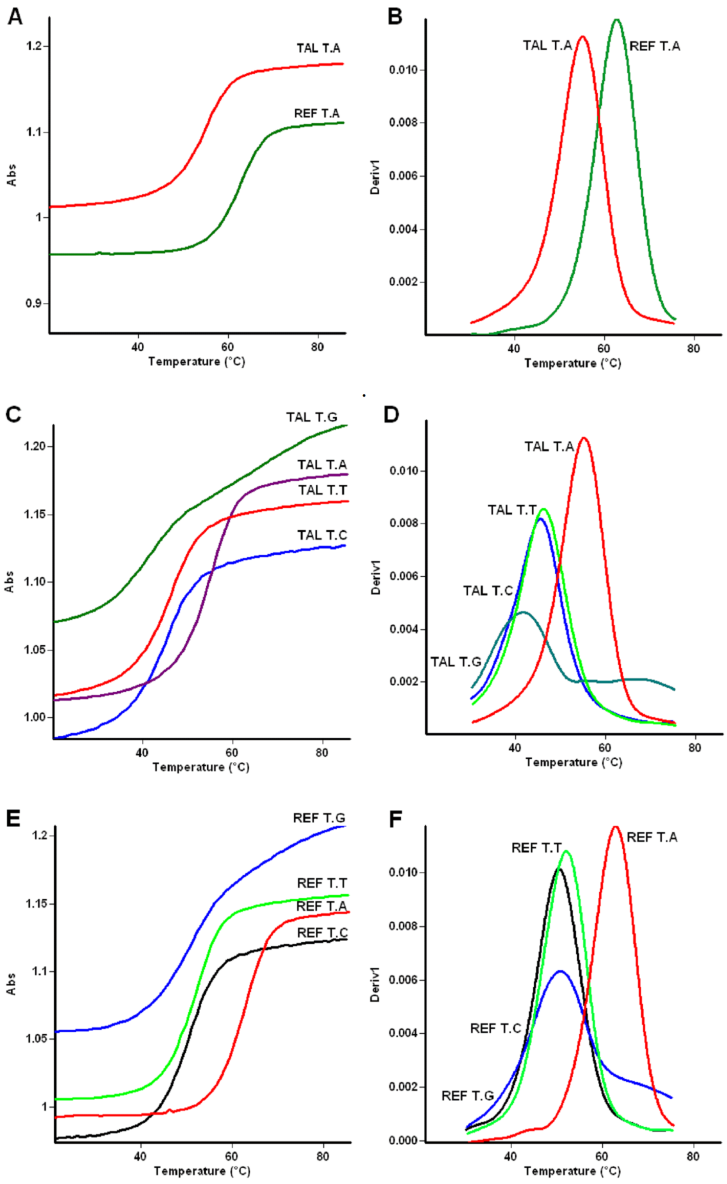

Fig. S4: *UV melting curves and derivatives of: 13merRef T.A and 13merTAL T.A (A, B), 13merTAL T.A and mismatches (C, D), 13merRef T.A and mismatches (E, F).*

Sequence of duplex	Base pair In 13-mer	T_m °C	Δ T_m °C	hyper chromicity %	Δ hyper chromicity %
5′-CGACG**T**TTGCAGC 3′-GCTGC**A**AACGTCG	REF T.A Watson-Crick	62.89 (0.13)	+7.59	15.57 (0.14)	–4.7
5′-CGACG**T**$_t$TTGCAGC 3′-GCTGC**A** AACGTCG	TAL T.A Watson-Crick	55.30 (0.10)	-	16.34 (0.08)	-
5′-CGACG**T**$_t$TTGCAGC 3′-GCTGC**C** AACGTCG	TAL T.C mismatch	45.31 (0.25)	–9.99	13.83 (0.11)	–15.4
5′-CGACG**T**$_t$TTGCAGC 3′-GCTGC**G** AACGTCG	TAL T.G mismatch	41.36 (0.32)	–13.94	12.53 (0.11)	–23.3
5′-CGACG**T**$_t$TTGCAGC 3′-GCTGC**T** AACGTCG	TAL T.T mismatch	46.44 (0.15)	–8.86	13.43 (0.13)	–17.8
Average for TAL mismatches			–10.9		–18.8

Table S1: *Ultraviolet melting studies on 13merRef, 13merTAL and mismatched 13merTAL duplexes.*

The base opposite to the thymine base at the 5'-side of the triazole linkage is varied: t = triazole linkage. ΔT_m = (T_m - T_m of TAL T.A)
Δhyperchromicity % = ((hyperchromicity - hyperchromicity of 13merTAL)/hyperchromicity of 13merTAL) x 100. This gives the percentage difference in hyperchromicity between 13merTAL and the other duplexes. Standard deviations are in parenthesis. The results are derived from 6 melting curves and 6 annealing curves for all samples.

Sequence of duplex	Base pair In 13-mer	T_m °C	Δ T_m °C	hyper chromicity %	Δ hyper chromicity %
5′-CGACG**T**TTGCAGC 3′-GCTGC**A**AACGTCG	REF T.A Watson-Crick	62.89 (0.13)	-	15.57 (0.14)	-
5′-CGACG**T**TTGCAGC 3′-GCTGC**C**AACGTCG	REF T.C mismatch	50.75 (0.18)	–12.14	14.79 (0.05)	–5.00
5′-CGACG**T**TTGCAGC 3′-GCTGC**G**AACGTCG	REF T.G mismatch	50.92 (0.12)	–11.97	13.80 (0.11)	–11.37
5′-CGACG**T**TTGCAGC 3′-GCTGC**T**AACGTCG	REF T.T mismatch	52.14 (0.15)	–10.75	14.62 (0.13)	–6.10
Average for REF mismatches			–11.6		–7.49

Table S2: *Ultraviolet melting studies on 13merRef and mismatched 13merRef duplexes.*

The base opposite to the thymine base is varied: ΔT_m = (T_m - T_m of Ref T.A)
Δhyperchromicity % = ((hyperchromicity - hyperchromicity of 13merRef)/hyperchromicity of 13merRef) x 100. This gives the percentage difference in hyperchromicity between 13merRef and the other duplexes. Standard deviations are in parenthesis. The results are derived from 3 melting curves and 3 annealing curves for all samples.

3 Chemical shifts: assignment, comparison, interpretation

The NOESY-spectra were assigned with the sequential approach [S1,S2]. Cross peaks expected for a regular B-DNA helix are all present in the NOESY-spectra of both samples. Based on the assignment of the H1' and H6/H8 protons, the remaining base and sugar protons could be assigned by combining the information from the COSY-, TOCSY-, HMQC-, and NOESY-spectra. Assignment of the exchangeable protons was done in the *WATERGATE-NOESY*-spectrum. The imino proton of T20 was easily identified because of the symmetry of the sequence, but the remaining imino, amino, and H2 protons had to be referenced to the already assigned non-exchangeable H5 protons via the H42/H41-H5 NOE cross-peaks. For the Triazole backbone modification the following chemical shifts were measured and unambiguously assigned: C1A=63.7 ppm, C3A=124.4 ppm, C7A=51.8 ppm, H1A=4.75 ppm, H1B=5.12 ppm, H3A=8.32 ppm, H7A=4.68 ppm, H1A=5.00 ppm. ^{1}H Chemical Shift Differences (CSDs) between 13merRef and 13merTAL are negligible for all base pairs that are not linked via the triazole. There is no significant trend that either 3'- or 5'- neighbours exhibit larger CSDs.

NMR measurements for structure calculation were carried out on a Bruker Avance 600. The optimum temperature of 298 K was determined by monitoring the imino proton signal intensity. For each duplex, NOESY-, DQF-COSY-, TOCSY- and HMQC-spectra in D_2O, a WATERGATE-NOESY-spectrum in H_2O and an HMQC-spectrum in D_2O/Pf1-phage were recorded. The quadrupolar splitting of the ^{2}H NMR signal after addition of Pf1-phage was 15.66 Hz for 13merTAL. For DQF-COSY- (TOCSY-) spectra, 16 (32) transients were acquired, with 2048×256 points in F2 and F1 dimensions. For NOESY-spectra in both solvents, 16 transients were acquired with 4096×2048 points at a mixing time of 150 ms. For the HMQC-spectra with and without Pf1-phage, 192 transients were acquired with 8192×512 points; the optimal d2-delay was 2.5 ms. All spectra were processed with the Bruker Topspin-software, and signals were assigned with the help of Cara [S3].

The ^{31}P-spectra of 13merRef and 13merTal are compared. No significant chemical shifts of the phosphate backbone atoms is observed. This is in line with the results from the structure calculations which suggest only minor changes in the phosphate backbone conformation consistent with standard B-type helices.

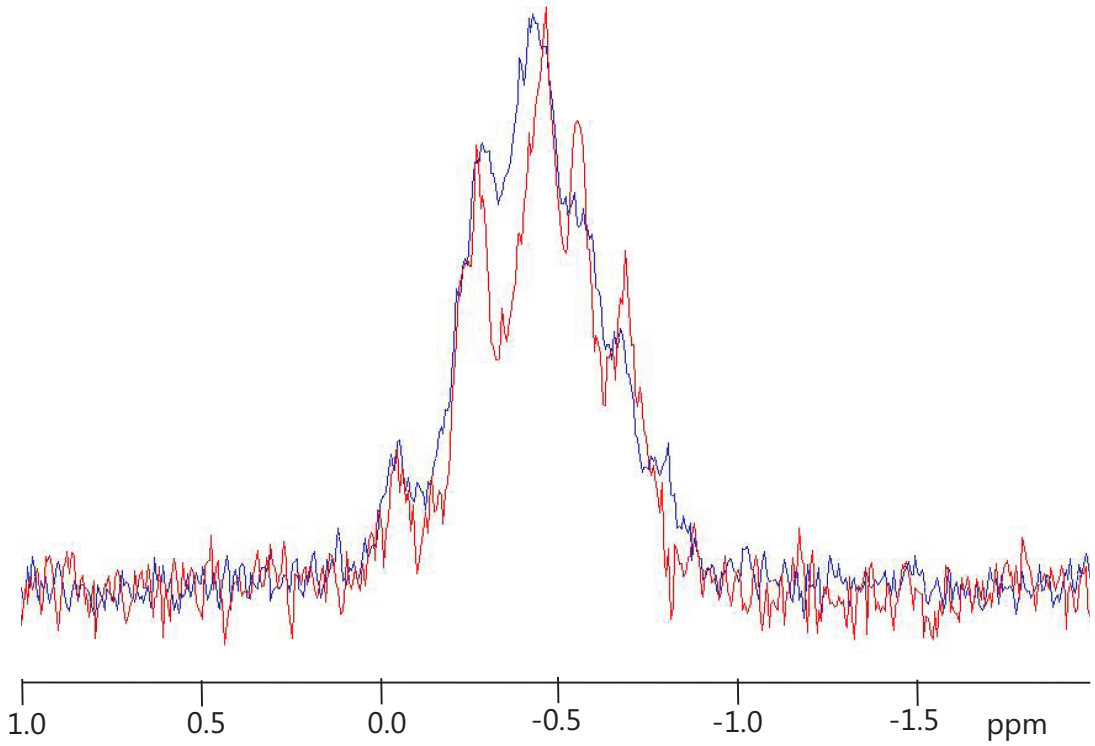

Fig. S5: ^{31}P*-spectra of 13merRef (red) and 13merTal (blue)*

Table S3: ^{1}H *chemical shifts of sugar protons of 13merRef*

Res	H1'	H2'	H2"	H3'	H4'
G1	6.02	2.68	2.81	4.87	4.28
C2	6.11	2.15	2.55	4.86	4.28
T3	5.76	2.15	2.47	4.90	4.17
G4	5.86	2.63	2.70	4.99	4.38
C5	5.41	1.84	2.22	4.79	4.11
A6	5.75	2.71	2.84	5.03	4.36
A7	5.84	2.63	2.84	5.05	4.43
A8	6.05	2.54	2.83	5.00	4.44
C9	5.56	1.92	2.32	4.77	4.14
G10	5.95	2.61	2.78	4.95	4.36
T11	6.05	2.10	2.47	4.88	4.23
C12	5.72	2.03	2.38	4.85	4.14
G13	6.18	2.64	2.40	4.70	4.20
C14	5.73	1.87	2.37	4.70	4.07
G15	5.46	2.73	2.80	5.01	4.33
A16	6.27	2.71	2.92	5.08	4.49
C17	5.56	1.99	2.36	4.82	4.17
G18	6.00	2.62	2.82	4.96	4.39
T19	6.04	2.14	2.61	4.87	4.28
T20	6.13	2.17	2.62	4.91	4.19
T21	5.84	2.10	2.48	4.91	4.15
G22	5.82	2.65	2.67	5.00	4.38
C23	5.49	1.98	2.32	4.83	4.16
A24	6.01	2.74	2.89	5.04	4.38
G25	5.82	2.48	2.66	4.96	4.36
C26	6.13	2.14	2.20	4.47	4.05

Table S4: *^{1}H chemical shifts of base protons of 13merRef*

Res	H1	H2	H3	H41	H42	H5	H6	H7	H8
G1	-	-	-	-	-	-	-	-	7.99
C2	-	-	-	8.33	6.62	5.39	7.55	-	-
T3	-	-	13.95	-	-	-	7.36	1.66	-
G4	12.71	-	-	-	-	-	-	-	7.89
C5	-	-	-	8.34	6.31	5.40	7.30	-	-
A6	-	7.17	-	-	-	-	-	-	8.19
A7	-	7.13	-	-	-	-	-	-	8.11
A8	-	7.58	-	-	-	-	-	-	8.05
C9	-	-	-	7.91	6.36	5.10	7.12	-	-
G10	12.67	-	-	-	-	-	-	-	7.81
T11	-	-	13.75	-	-	-	7.27	1.39	-
C12	-	-	-	8.62	7.02	5.72	7.51	-	-
G13	-	-	-	-	-	-	-	-	7.97
C14	-	-	-	-	-	5.91	7.62	-	-
G15	12.95	-	-	-	-	-	-	-	7.97
A16	-	7.91	-	-	-	-	-	-	8.23
C17	-	-	-	8.11	6.44	5.23	7.21	-	-
G18	12.76	-	-	-	-	-	-	-	7.83
T19	-	-	13.91	-	-	-	7.25	1.37	-
T20	-	-	13.90	-	-	-	7.47	1.62	-
T21	-	-	13.70	-	-	-	7.33	1.69	-
G22	12.60	-	-	-	-	-	-	-	7.89
C23	-	-	-	8.32	6.34	5.39	7.37	-	-
A24	-	7.66	-	-	-	-	-	-	8.19
G25	12.94	-	-	-	-	-	-	-	7.69
C26	-	-	-	-	-	5.33	7.38	-	-

Table S5: *^{13}C chemical shifts of 13merRef*

Res	C1'	C3'	C2	C5	C6	C8
G1	82.2	75.3	-	-	-	135.9
C2	83.9	76.6	-	95.7	140.1	-
T3	82.8	75.3	-	-	136.6	-
G4	81.4	76.5	-	-	-	135.5
C5	83.3	76.1	-	95.5	139.6	-
A6	81.7	76.9	151.4	-	-	138.7
A7	82.2	76.1	151.1	-	-	138.2
A8	81.9	76.6	152.0	-	-	138.0
C9	83.1	74.0	-	95.1	139.1	-
G10	82.0	76.9	-	-	-	135.5
T11	82.7	75.1	-	-	135.8	-
C12	83.8	76.5	-	96.1	141.0	-
G13	82.0	70.6	-	-	-	135.5
C14	85.2	75.1	-	96.8	140.4	-
G15	81.3	76.7	-	-	-	136.4
A16	82.1	76.9	152.7	-	-	138.4
C17	83.2	74.0	-	95.4	139.2	-
G18	82.1	75.2	-	-	-	135.5
T19	82.7	75.1	-	-	135.8	-
T20	82.7	74.8	-	-	137.2	-
T21	81.5	74.7	-	-	136.7	-
G22	81.3	76.6	-	-	-	135.5
C23	83.5	75.3	-	95.5	139.9	-
A24	82.1	77.0	151.5	-	-	138.8
G25	81.2	75.0	-	-	-	134.5
C26	84.0	68.8	-	95.3	140.2	-

Table S6: ^{1}H *chemical shifts of sugar protons of 13merTAL*

Res	H1'	H2'	H2"	H3'	H4'
G1	6.00	2.68	2.80	4.87	4.29
C2	6.10	2.15	2.55	4.87	4.28
T3	5.77	2.16	2.48	4.91	4.17
G4	5.86	2.65	2.71	5.00	4.38
C5	5.43	1.89	2.26	4.80	4.14
A6	5.88	2.71	2.88	5.04	4.38
A7	5.80	2.59	2.81	5.04	4.42
A8	6.05	2.53	2.82	4.99	4.43
C9	5.52	1.89	2.30	4.78	4.11
G10	5.94	2.62	2.78	4.96	4.36
T11	6.05	2.09	2.47	4.88	4.23
C12	5.72	2.04	2.39	4.87	4.15
G13	6.18	2.66	2.42	4.71	4.21
C14	5.72	1.85	2.36	4.70	4.08
G15	5.45	2.74	2.81	5.02	4.33
A16	6.28	2.72	2.93	5.09	4.50
C17	5.56	2.02	2.37	4.84	4.19
G18	6.04	2.64	2.87	5.01	4.42
T19	5.85	1.71	1.55	4.54	4.07
T20	5.76	1.94	2.77	4.79	4.17
T21	5.86	2.19	2.55	4.93	4.23
G22	5.82	2.63	2.69	5.01	4.37
C23	5.49	1.99	2.33	4.84	4.17
A24	6.01	2.74	2.90	5.05	4.39
G25	5.82	2.48	2.66	4.97	4.38
C26	6.11	2.16	2.23	4.47	4.05

Table S7: ^{1}H *chemical shifts of base protons of 13merTAL*

Res	H1	H2	H3	H41	H42	H5	H6	H7	H8
G1	-	-	-	-	-	-	-	-	7.98
C2	-	-	-	8.39	6.69	5.37	7.55	-	-
T3	-	-	13.99	-	-	-	7.36	1.67	-
G4	12.74	-	-	-	-	-	-	-	7.91
C5	-	-	-	8.34	6.39	5.41	7.33	-	-
A6	-	7.24	-	-	-	-	-	-	8.16
A7	-	7.08	-	-	-	-	-	-	8.03
A8	-	7.51	-	-	-	-	-	-	8.02
C9	-	-	-	7.97	6.36	5.11	7.08	-	-
G10	12.71	-	-	-	-	-	-	-	7.82
T11	-	-	13.76	-	-	-	7.26	1.40	-
C12	-	-	-	8.66	7.06	5.72	7.51	-	-
G13	-	-	-	-	-	-	-	-	7.96
C14	-	-	-	8.19	7.06	5.88	7.60	-	-
G15	12.98	-	-	-	-	-	-	-	7.97
A16	-	7.94	-	-	-	-	-	-	8.24
C17	-	-	-	8.11	6.47	5.25	7.24	-	-
G18	12.71	-	-	-	-	-	-	-	7.87
T19	-	-	13.73	-	-	-	7.24	1.37	-
T20	-	-	13.95	-	-	-	7.00	1.63	-
T21	-	-	13.81	-	-	-	7.49	1.75	-
G22	12.61	-	-	-	-	-	-	-	7.90
C23	-	-	-	8.36	6.38	5.39	7.38	-	-
A24	-	7.69	-	-	-	-	-	-	8.19
G25	12.98	-	-	-	-	-	-	-	7.68
C26	-	-	-	-	-	5.23	7.33	-	-

Table S8: *^{13}C chemical shifts of 13merTAL*

Res	C1'	C3'	C2	C5	C6	C8
G1	82.3	75.3	-	-	-	136.4
C2	84.1	76.6	-	95.7	140.1	-
T3	82.9	75.3	-	-	136.6	-
G4	81.4	76.5	-	-	-	135.5
C5	83.3	76.1	-	95.5	139.7	-
A6	81.7	76.9	151.3	-	-	138.8
X7	81.5	76.1	151.0	-	-	138.1
A8	81.9	76.6	151.9	-	-	138.0
C9	83.1	74.0	-	95.2	139.0	-
G10	82.0	76.9	-	-	-	135.5
T11	82.7	75.1	-	-	135.8	-
C12	83.8	76.5	-	96.1	141.0	-
G13	82.2	70.6	-	-	-	135.5
C14	85.1	75.1	-	96.6	140.3	-
G15	81.3	76.7	-	-	-	136.4
A16	82.1	76.9	152.6	-	-	138.3
C17	83.2	74.0	-	95.4	139.3	-
G18	82.1	75.2	-	-	-	135.7
T19	82.8	78.6	-	-	135.9	-
T20	86.1	74.8	-	-	134.9	-
T21	82.9	74.7	-	-	137.0	-
G22	81.3	76.6	-	-	-	135.5
C23	83.5	75.3	-	95.5	139.9	-
A24	82.1	77.0	151.5	-	-	138.8
G25	81.2	75.0	-	-	-	134.5
C26	84.0	68.8	-	95.0	140.2	-

Table S9: ^{1}H *chemical shift differences for 13merRef and 13merTAL.*

Res	H1'	H2'	H2"	H3'	H4'	H1/H3 H41/H42	H2/H5 H7	H6/H8
G1	-0.02	0.00	-0.01	0.01	0.01	-	-	-0.01
C2	0.00	0.00	0.00	0.00	0.00	0.06/0.07	-0.01	-0.01
T3	0.01	0.01	0.01	0.01	0.01	0.04	0.00	0.00
G4	0.00	0.02	0.01	0.01	0.01	0.03	-	0.01
C5	0.02	0.04	0.04	0.01	0.03	0.01/0.07	0.01	0.02
A6	0.12	0.00	0.04	0.01	0.02	-	0.07	-0.03
A7	-0.04	-0.04	-0.02	-0.01	-0.01	-	-0.05	-0.08
A8	0.00	-0.01	0.00	-0.01	-0.01	-	-0.07	-0.03
C9	-0.04	-0.03	-0.01	0.01	-0.03	0.06/0.00	0.01	-0.03
G10	-0.01	0.01	0.00	0.01	0.00	0.04	-	0.01
T11	-0.01	-0.01	0.00	0.00	0.00	0.01	0.02	-0.01
C12	0.00	0.01	0.00	0.01	0.01	0.03/0.03	0.00	0.00
G13	0.00	0.01	0.02	0.01	0.01	-	-	-0.01
C14	-0.01	-0.02	0.00	0.00	0.01	-	-0.03	-0.02
G15	-0.01	0.00	0.01	0.01	0.01	0.03	-	0.01
A16	0.01	0.01	0.01	0.01	0.01	-	0.02	0.01
C17	0.00	0.03	0.01	0.02	0.01	0.01/0.03	0.02	0.03
G18	0.03	0.02	0.05	0.05	0.03	-0.04	-	0.04
T19	-0.19	-0.42	-1.06	-0.33	-0.20	-0.18	0.00	-0.01
T20	-0.38	-0.23	0.15	-0.12	-0.02	0.04	0.01	-0.47
T21	0.02	0.09	0.07	0.02	0.08	0.11	0.06	0.17
G22	0.01	-0.02	0.02	0.01	-0.01	0.00	-	0.01
C23	0.00	0.01	0.01	0.01	0.01	0.03/0.03	0.00	0.01
A24	0.00	0.00	0.01	0.01	0.01	-	0.03	0.00
G25	0.00	0.00	0.00	0.01	0.02	0.04	-	-0.01
C26	-0.02	0.02	0.03	0.00	0.00	-	-0.11	-0.05

4 Structure calculation for 13merTAL and the reference duplex 13mer-Ref

The chemical structure and full labelling of the triazole linker as used in the structure calculation is depicted in Fig. S6. The labelling follows the constituents of the triazole linker, namely the propargyl and the azide groups.

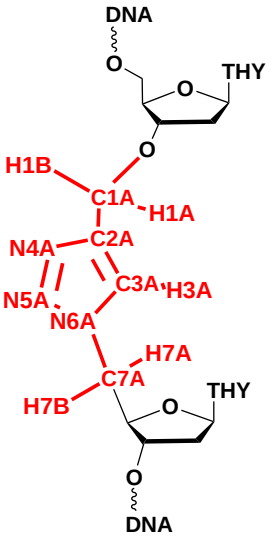

Fig. S6: *Chemical structure and full labelling of the triazole linker as used in the structure calculation. The labelling follows the constituents of the triazole linker, namely the propargyl group and the azide group.*

After hybridization the samples were subjected to size exclusion chromatography and ammonia treatment to remove residual, low molecular weight impurities (mainly Et_3N-buffer from HPLC). Samples were prepared at 3 mM concentration in D_2O (D_2O 99.98 %) and H_2O (H_2O:D_2O/90:10) at pH 6.5 in 10 mM Na_2HPO_4/NaH_2PO_4 and 150 mM NaCl solution. Samples for measuring residual dipolar couplings (RDC) were prepared in D_2O as described above with the addition of 20 mg/ml Pf1-phage.

NMR measurements for structure calculation were carried out on a Bruker Avance 600. The optimum temperature of 298 K was determined by monitoring the imino proton signal intensity. For each duplex, NOESY-, DQF-COSY-, TOCSY- and HMQC-spectra in D_2O, a WATERGATE-NOESY-spectrum in H_2O and an HMQC-spectrum in D_2O/Pf1-phage were recorded. The quadrupolar splitting of the ^2H NMR signal after addition of Pf1-phage was 15.66 Hz for 13merTAL. For DQF-COSY- (TOCSY-) spectra, 16 (32) transients were acquired, with 2048×256 points in F2 and F1 dimensions. For NOESY-spectra in both solvents, 16 transients were acquired with 4096×2048 points at a mixing time of 150 ms. For the HMQC-spectra with and without Pf1-phage, 192 transients were acquired with 8192×512 points; the optimal d2-delay was 2.5 ms. All spectra were processed with the Bruker Topspin-software, and signals were assigned with the help of Cara [S3].

The assigned NOE cross-peaks were converted to distance restraints by referencing their integrals to integrals of known distances employing the Isolated Spin Pair Approximation. The NOE cross-peaks were integrated with the program Cara [S3]. As reference distances we used Me-H6 T (3.1 Å) for all NOE cross-peaks involving methyl protons, H42-H5 C (2.4 Å) for all NOE cross-peaks involving exchangeable protons and H5-H6 C (2.5 Å) for the remaining NOE cross-peaks.

The distance restraints were used together with standard B-DNA dihedral restraints for the phosphate backbone, since all H1'-H2' dipolar couplings were estimated in the range of 8-10 Hz, which is typical for standard B-DNA. Additionally, planarity and hydrogen bond restraints were included to perform Simulated Annealing calculations. For structural statistics see Table S10.

Structure calculations were performed with Xplor-NIH v2.20 [S4]. Force field parameters for the TAL linker were obtained by DFT calculations performed with Gaussian03, TZVP basis set, and the CHelpG algorithm to derive atomic charges via the Molecular Electrostatic Potential. [S5] A total of 351 NOE distance restraints and 39

Residual Dipolar Couplings were used for 13merTAL. The experimental data were supplemented with 136 backbone dihedral restraints, 78 hydrogen bond distance restraints and 28 planarity restraints

Table S10: *Overview of the structural statistics for 13merRef and 13merTAL*

	13merRef	**13merTAL**
NOE restraints		
- total	340	351
- interresidue	196	208
- intraresidue	144	143
- TAL to DNA	-	14
RDC restraints	24	39
Dihedral angle restr.	144	136
H-bond restr.	78	78
Bp planarity restr.	28	28
NOE viol. (> 0.5 Å)	0	0
RDC viol. (> 0.4 Hz)	0	0
Dihe viol. (> 5 Â°)	0	0
RMSD to ave. struct. in Å	0.30	0.37

The structures were calculated in two steps with XPLOR-NIH v2.20 [S4]. First, a reasonable starting structure with well defined local conformation was computed. We started from an elongated and equilibrated structure to ensure that no bias is introduced towards local energy minima. The resulting structure, which is mainly defined by NOE restraint data, was used as input for Simulated Annealing calculations including RDC data. The need for locally well defined starting structures in order to calculate reasonable structures which satisfy NOE as well as RDC data is documented in the literature [S6, S7].

The MD protocol with only NOE restraints as experimental input data consisted of an initial minimization (50 steps) followed by 48 ps of high-temperature cartesian coordinate dynamics at 3000 K, subsequent gradual cooling to 25 K in 120 steps and a final minimization (3000 steps).

The MD protocol including the additional RDC restraints consisted of an initial cartesian coordinate minimization (1000 steps) followed by 50 ps of high-temperature torsion angle dynamics at 20000 K, subsequent gradual cooling to 25 K in 154 steps of 0.5 ps length (34 steps to cool down to 3000 K, followed by 120 steps to reach the end temperature) and a final minimization (3000 steps). The experimentally determined C-H RDCs for the T methyl groups were converted to the respective C-C RDCs using the factor -0.3155 [S8] automatically by an updated version of the corresponding XPLOR-NIH v2.20-routine. Since the RDC-energy is related to the square of the RDC-value, the energy of the methyl-RDCs has to be scaled by $(-0.3155)^2$=0.0995. The alignment tensor values were allowed to float during the calculations, as implemented in XPLOR-NIH v2.20 [S4].

For each run an ensemble of 100 structures was computed. The 10 minimum energy structures without violation of restraints were chosen to compute an averaged structure which was energy-minimized to yield the final structure (cf. Fig. S7).

To improve the accuracy of the structures, NOESY-spectra were back-calculated from the average structures with the Full Matrix Relaxation Approach implemented in XPLOR-NIH v2.20 [S4]. The back-calculated spectra were visualized with the program GIFA [S9] and overlayed with the experimental ones (Fig. S9a and S9b). The back-calculated and the experimental spectrum are in good agreement with each other for 13merRef as well as 13merTAL. Furthermore, RDCs were predicted from the average structure. These were compared with the experimental ones, yielding correlation factors (R) of 1.000 and q-factors of 0.003 and 0.006 for 13merRef and 13merTAL respectively. The correlation plots of experimentally determined and predicted RDCs are shown in Fig. S8a and S8b.

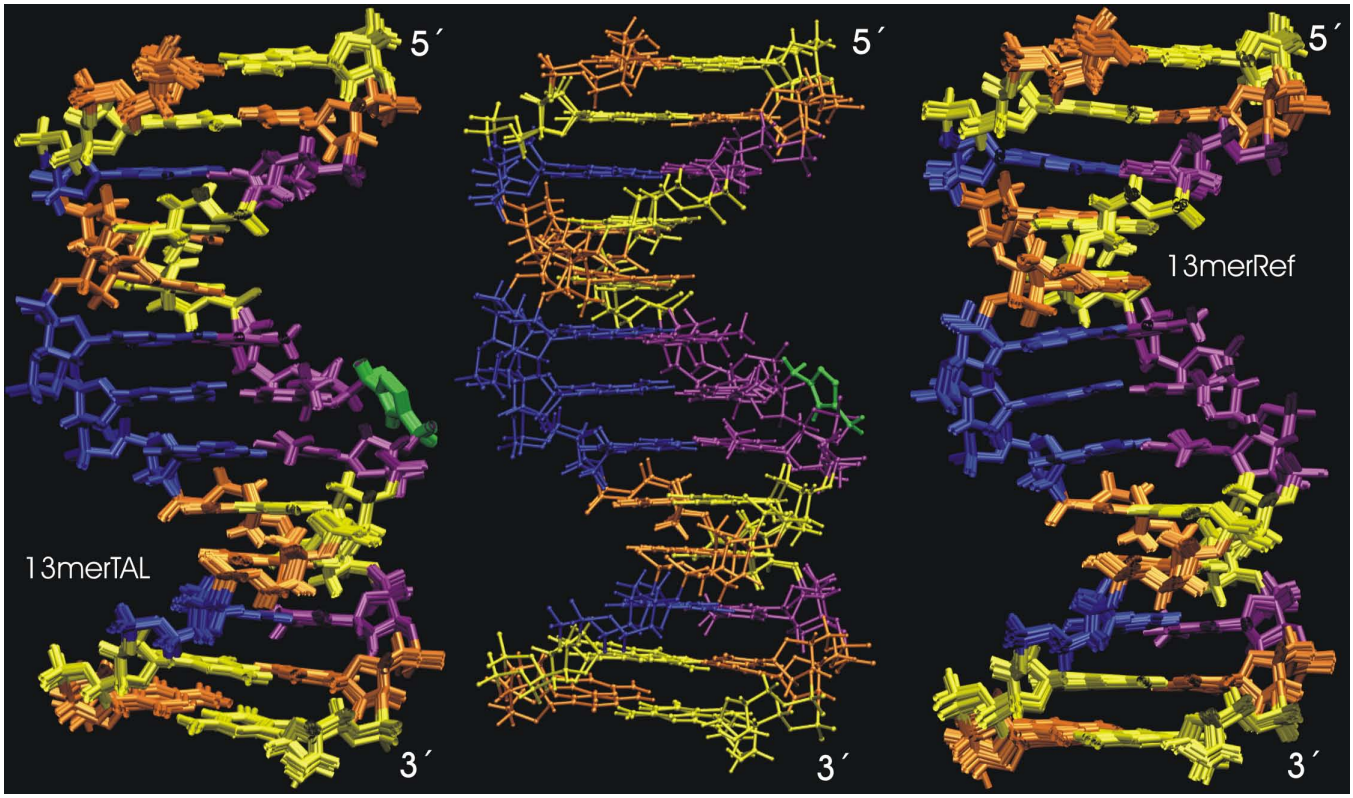

Fig. S7: *Overlay (centre) of the average of the 10 best-energy, violation-free structures for 13merRef (right) and 13merTAL (left). The triazole is shown in green.*

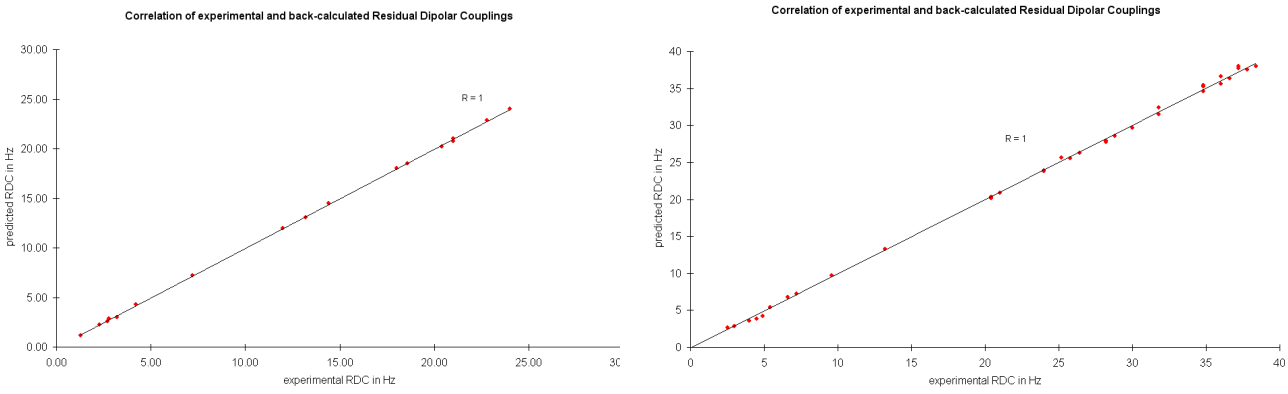

(a) *13merRef* **(b)** *13merTAL*

Fig. S8: *Plot of the experimental vs predicted Residual Dipolar Couplings for 13merRef and 13merTAL.*

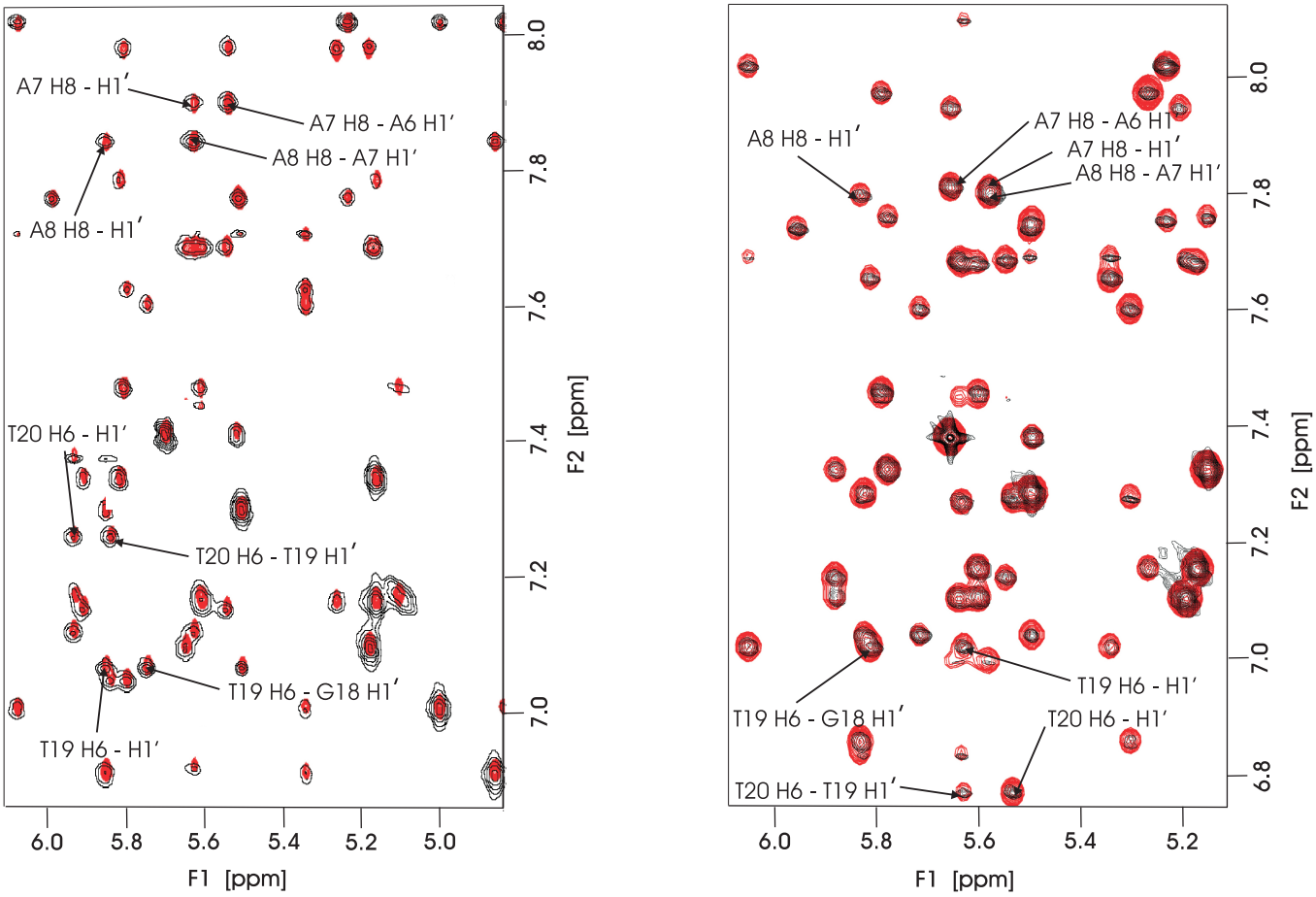

(a) *13merRef* **(b)** *13merTAL*

Fig. S9: *Overlay of the experimental NOESY spectrum at 150 ms mixing time (green) and the NOESY spectrum back-calculated from the average structure of the 10 lowest energy and violation-free structures, as obtained by restrained molecular dynamics calculations in* XPLOR-NIH v2.20 *[S4] (red). Arrows point to NOE cross-peaks involving the modification site.*

5 Experimental Residual Dipolar couplings for 13merRef and 13merTAL

Table S11: *Experimentally determined Residual Dipolar Couplings for 13merRef. The Residual Dipolar Couplings were measured with a precision of ±0.6 Hz.*

Res	Vektor	$J_{(CH)}$ (Hz)	$J_{(CH)}$(aligned) (Hz)	Residual Dipolar coupling (Hz)
A6	C2-H2	201.6	225.6	24.0
A7	C2-H2	203.4	224.4	21.0
A8	C2-H2	202.2	223.8	21.6
A16	C2-H2	202.8	214.8	12.0
A24	C2-H2	201.6	224.4	22.8
C9	C5-H5	171.6	190.2	18.6
C17	C5-H5	170.4	183.6	13.2
T3	C7-H7	126.6	122.4	-4.2
T11	C7-H7	126.0	118.8	-7.2
T19	C7-H7	123.0	112.8	-10.2
T20	C7-H7	127.2	118.2	-9.0
T21	C7-H7	126.6	118.2	-8.4
T3	C1'-H1'	155.4	167.4	12.0
C9	C1'-H1'	162.0	169.2	7.2
C17	C1'-H1'	162.6	166.8	4.2
T20	C1'-H1'	163.8	178.2	14.4
T21	C1'-H1'	153.6	174.0	20.4
T3	C6-H6	177.0	195.0	18.0
C5	C6-H6	180.0	201.0	21.0
T20	C6-H6	177.0	192.6	15.6
T21	C6-H6	175.8	190.8	15.0
C23	C6-H6	175.8	201.0	25.2
A7	C8-H8	213.0	235.8	22.8
A16	C8-H8	213.0	230.4	17.4

Table S12: *Experimentally determined Residual Dipolar Couplings for 13merTAL. The Residual Dipolar Couplings were measured with a precision of ±0.6 Hz.*

Res	Vektor	$J_{(CH)}$ (Hz)	$J_{(CH)}$(aligned) (Hz)	Residual Dipolar coupling (Hz)
ADE 6	C2-H2	201.6	238.2	36.6
ADE 7	C2-H2	202.8	232.8	30.0
ADE 8	C2-H2	202.8	231.0	28.2
ADE 16	C2-H2	202.8	223.8	21.0
ADE 24	C2-H2	201.6	237.6	36.0
CYT 5	C5-H5	169.2	193.2	24.0
CYT 23	C5-H5	169.2	193.2	24.0
THY 3	C7-H7	127.2	117.6	-9.6
THY 11	C7-H7	127.2	112.8	-14.4
THY 19	C7-H7	127.2	114.6	-12.6
TAL 20	C7-H7	127.2	111.6	-15.6
THY 21	C7-H7	127.2	119.4	-7.8
THY 3	C1'-H1'	166.8	172.2	5.4
CYT 5	C1'-H1'	165.6	175.2	9.6
THY 11	C1'-H1'	164.4	171.6	7.2
THY 19	C1'-H1'	162.0	182.4	20.4
TAL 20	C1'-H1'	171.0	155.4	-15.6
THY 21	C1'-H1'	162.0	182.4	20.4
CYT 23	C1'-H1'	162.6	175.8	13.2
THY 3	C6-H6	175.8	207.6	31.8
CYT 5	C6-H6	173.4	209.4	36.0
CYT 9	C6-H6	173.4	211.2	37.8
THY 11	C6-H6	177.0	203.4	26.4
CYT 17	C6-H6	175.8	214.2	38.4
THY 19	C6-H6	176.4	205.2	28.8
TAL 20	C6-H6	176.4	202.2	25.8
THY 21	C6-H6	174.6	202.8	28.2
CYT 23	C6-H6	172.2	207.0	34.8
GUA 4	C8-H8	215.4	252.6	37.2
ADE 6	C8-H8	214.8	246.6	31.8
ADE 7	C8-H8	213.6	248.4	34.8
ADE 8	C8-H8	213.6	248.4	34.8
ADE 16	C8-H8	213.6	238.8	25.2
GUA 18	C8-H8	213.6	249.6	36.0
GUA 22	C8-H8	215.4	252.6	37.2
ADE 24	C8-H8	211.8	246.6	34.8
TAL 20	C1A-H1B	160.2	151.8	-8.4
TAL 20	C3A-H3A	197.4	204.0	6.6
THY 19	C2'-H2"	133.8	128.4	-5.4

6 Helical parameters of the average structures of 13merRef and 13merTAL and their comparison

Analysis of the structures of 13merTAL and its reference (13merRef) show differences in their helical parameters. The helical parameters affected most by the substitution are “shift”, “slide”, “stagger” and “propeller twist”. The differences are most severe for the two base pairs that are linked via the triazole, and less striking for the adjacent ones.
vspace3cm

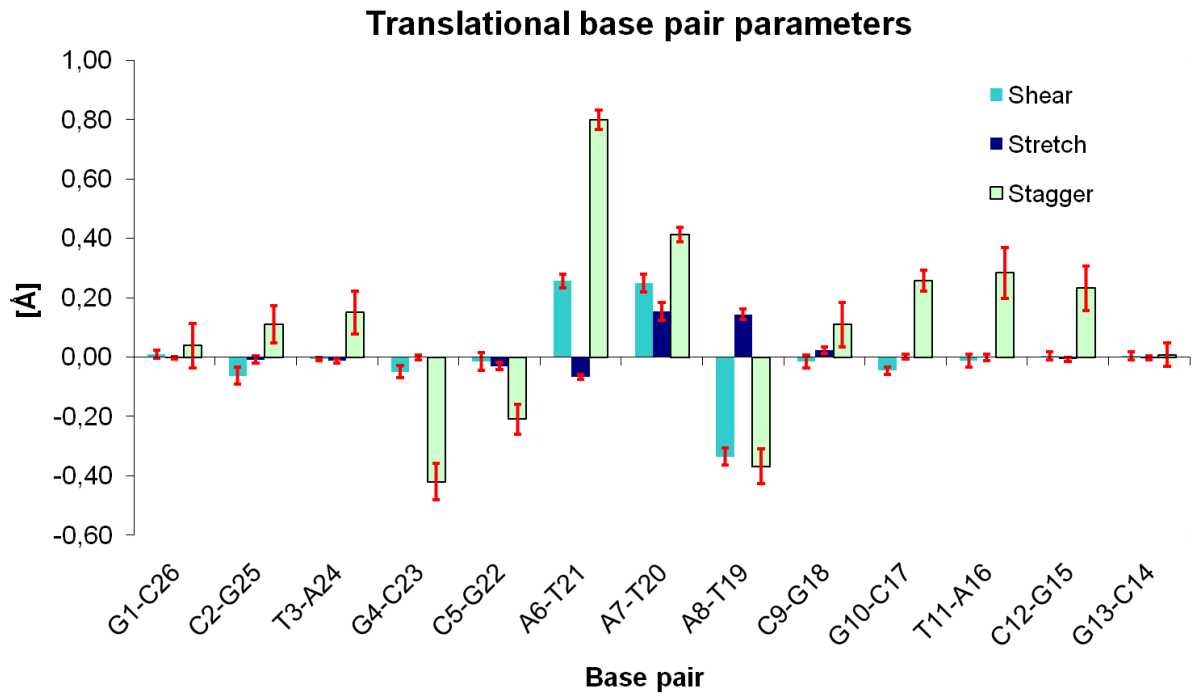

Fig. S10: *Plot of the deviations in helical parameters “shear”, “stretch” and “stagger” between 13merRef and 13merTAL with corresponding standard deviation within one ensemble (red error bars).*

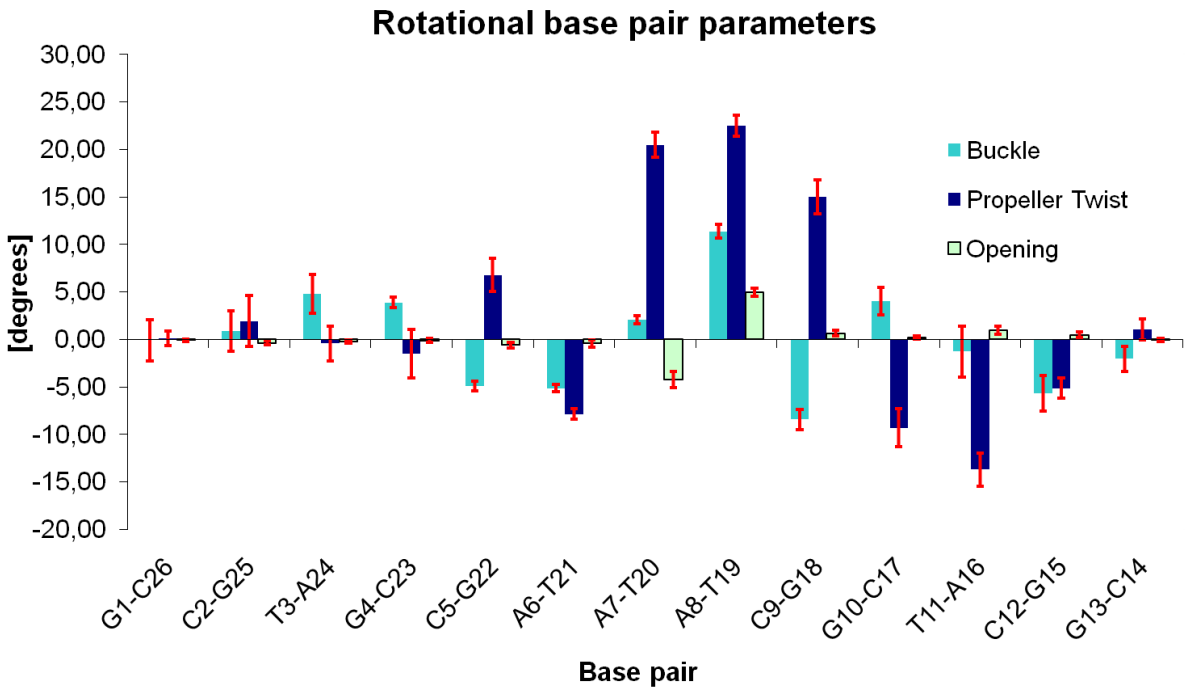

Fig. S11: *Plot of the deviations in helical parameters "buckle", "propeller twist" and "opening" between 13merRef and 13merTAL with corresponding standard deviation within one ensemble (red error bars).*

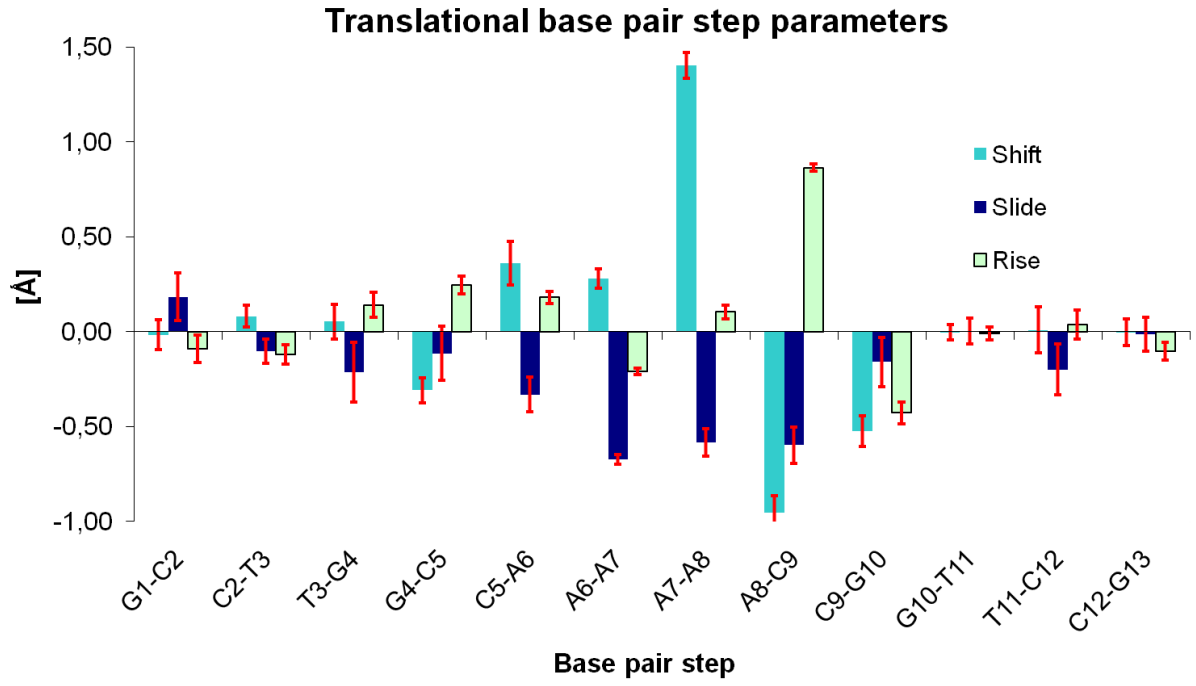

Fig. S12: *Plot of the deviations in helical parameters "shift", "slide" and "rise" between 13merRef and 13merTAL with corresponding standard deviation within one ensemble (red error bars).*

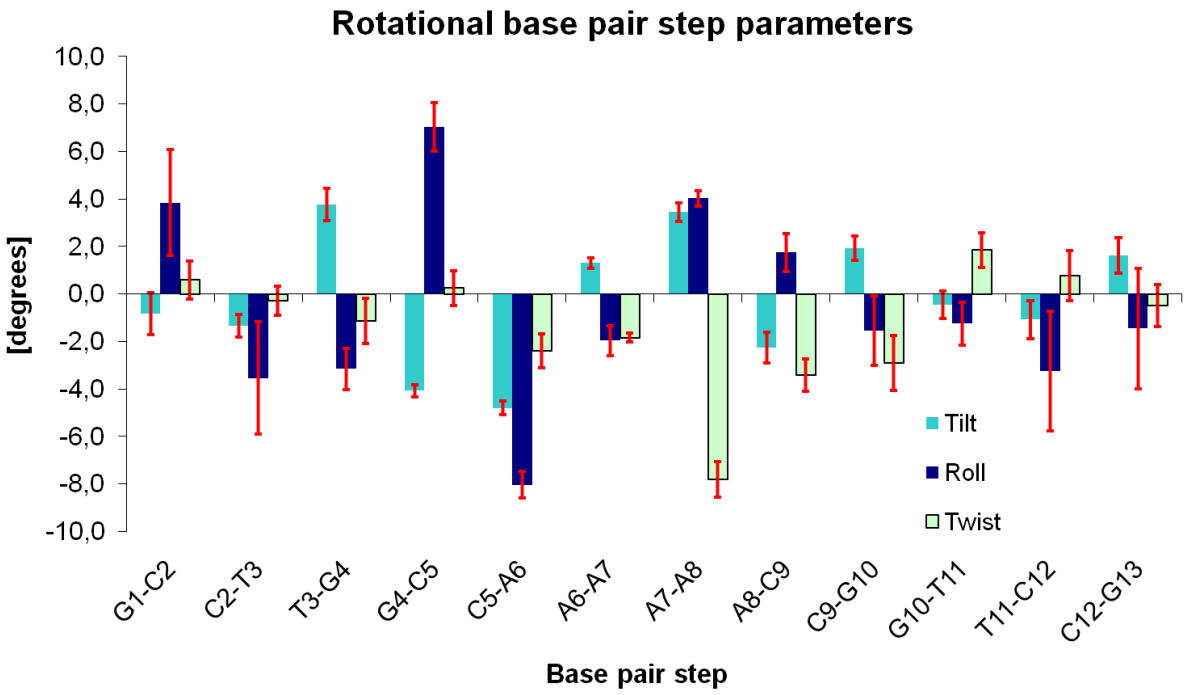

Fig. S13: *Plot of the deviations in helical parameters "tilt", "roll" and "twist" between 13merRef and 13merTAL with corresponding standard deviation within one ensemble (red error bars).*

Table S13: *Translational base pair parameters (average value) for 13merRef*

base pair	Shear (Sx)/Å	Stretch (Sy)/Å	Stagger (Sz)/Å
G1–C26	-0.42	-0.26	-0.14
C2–G25	0.42	-0.26	-0.13
T3–A24	-0.07	-0.26	0.07
G4–C23	-0.37	-0.28	0.10
C5–G22	0.40	-0.26	-0.13
A6–T21	0.02	-0.26	-0.04
A7–T20	0.07	-0.27	-0.24
A8–T19	0.03	-0.28	-0.06
C9–G18	0.39	-0.27	-0.05
G10–C17	-0.40	-0.26	0.08
T11–A16	-0.07	-0.27	0.09
C12–G15	0.40	-0.27	-0.11
G13–C14	-0.40	-0.26	-0.03

Table S14: *Rotational base pair parameters (average value) for 13merRef*

base pair	Buckle (χ)/Â°	Propeller Twist (ω)/Â°	Opening (σ)/Â°
G1–C26	-1.4	2.4	1.7
C2–G25	-4.7	3.8	1.5
T3–A24	-8.0	-1.8	-2.9
G4–C23	-0.4	5.4	1.5
C5–G22	5.3	3.5	1.6
A6–T21	6.3	-1.8	-2.9
A7–T20	4.9	-8.2	-2.5
A8–T19	5.1	-10.6	-2.7
C9–G18	4.3	-6.0	1.5
G10–C17	-1.2	1.2	1.5
T11–A16	2.6	-3.4	-3.0
C12–G15	4.6	-8.9	2.0
G13–C14	-0.6	-0.6	1.4

Table S15: *Translational base pair step parameters for (average value) 13merRef*

base pair step	Shift (Sx)/Å	Slide (Sy)/Å	Rise (Sz)/Å
G1–C2	-0.12	-0.71	3.40
C2–T3	-0.30	-1.35	3.38
T3–G4	0.44	-0.57	2.81
G4–C5	0.10	-0.25	3.06
C5–A6	-0.61	-0.67	3.01
A6–A7	-0.36	-0.87	3.27
A7–A8	-0.45	-0.66	3.11
A8–C9	-0.02	-0.72	3.20
C9–G10	0.17	-0.98	3.21
G10–T11	-0.23	-0.92	3.14
T11–C12	0.34	-0.28	3.00
C12–G13	0.02	-0.99	3.01

Table S16: *Rotational base pair step parameters (average value) for 13merRef*

base pair step	Tilt (τ)/Â°	Roll (ρ)/Â°	Twist (Ω)/Â°
G1–C2	-1.0	-4.9	41.1
C2–T3	1.6	-2.6	30.4
T3–G4	-0.6	3.7	35.2
G4–C5	2.1	2.1	40.6
C5–A6	-1.1	4.6	35.2
A6–A7	0.3	-2.4	33.4
A7–A8	-4.2	1.3	36.0
A8–C9	-2.7	-2.8	37.6
C9–G10	-2.3	0.7	33.3
G10–T11	1.8	-3.0	35.3
T11–C12	3.3	2.7	39.6
C12–G13	-1.0	10.0	30.6

Table S17: *Translational base pair parameters (average value) for 13merTAL*

base pair	Shear (Sx)/Å	Stretch (Sy)/Å	Stagger (Sz)/Å
G1–C26	-0.41	-0.26	-0.10
C2–G25	0.35	-0.27	-0.02
T3–A24	-0.08	-0.27	0.22
G4–C23	-0.42	-0.28	-0.32
C5–G22	0.39	-0.29	-0.34
A6–T21	0.28	-0.33	0.76
A7–T20	0.32	-0.12	0.17
A8–T19	-0.31	-0.13	-0.43
C9–G18	0.38	-0.25	0.06
G10–C17	-0.44	-0.26	0.34
T11–A16	-0.08	-0.27	0.37
C12–G15	0.41	-0.27	0.12
G13–C14	-0.39	-0.26	-0.02

Table S18: *Rotational base pair parameters (average value) for 13merTAL*

base pair	Buckle (χ)/Â°	Propeller Twist (ω)/Â°	Opening (σ)/Â°
G1–C26	-1.4	2.6	1.6
C2–G25	-3.9	5.8	1.2
T3–A24	-3.2	-2.2	-3.1
G4–C23	3.5	3.9	1.4
C5–G22	0.4	10.3	1.0
A6–T21	1.2	-9.7	-3.3
A7–T20	7.0	12.3	-6.7
A8–T19	16.4	11.9	2.3
C9–G18	-4.1	9.1	2.2
G10–C17	2.9	-8.1	1.7
T11–A16	1.3	-17.0	-2.1
C12–G15	-1.1	-14.0	2.5
G13–C14	-2.6	0.5	1.4

Table S19: *Translational base pair step parameters (average value) for 13merTAL*

base pair step	Shift (Sx)/Å	Slide (Sy)/Å	Rise (Sz)/Å
G1–C2	-0.13	-0.53	3.31
C2–T3	-0.22	-1.46	3.26
T3–G4	0.49	-0.78	2.95
G4–C5	-0.21	-0.36	3.31
C5–A6	-0.25	-1.00	3.19
A6–A7	-0.08	-1.54	3.06
A7–A8	0.95	-1.24	3.21
A8–C9	-0.97	-1.31	4.06
C9–G10	-0.35	-1.14	2.78
G10–T11	-0.23	-0.92	3.13
T11–C12	0.35	-0.48	3.04
C12–G13	0.02	-1.00	2.91

Table S20: *Rotational base pair step parameters (average value) for 13merTAL*

base pair step	Tilt (τ)/Â°	Roll (ρ)/Â°	Twist (Ω)/Â°
G1–C2	-1.8	-1.0	41.7
C2–T3	0.3	-6.1	30.1
T3–G4	3.2	0.5	34.0
G4–C5	-1.9	9.1	40.8
C5–A6	-5.9	-3.4	32.8
A6–A7	1.6	-4.3	31.5
A7–A8	-0.7	5.3	28.2
A8–C9	-5.0	-1.1	34.2
C9–G10	-0.4	-0.8	30.4
G10–T11	1.4	-4.3	37.2
T11–C12	2.2	-0.5	40.4
C12–G13	0.6	8.5	30.2

Table S21: *Differences in translational base pair parameters for 13merTAL and 13merRef*

base pair	Shear (Sx)/Å	Stretch (Sy)/Å	Stagger (Sz)/Å
G1–C26	0.01	-0.00	0.04
C2–G25	-0.06	-0.01	0.11
T3–A24	-0.01	-0.01	0.15
G4–C23	-0.05	-0.00	-0.42
C5–G22	-0.02	-0.03	-0.21
A6–T21	0.26	-0.07	0.80
A7–T20	0.25	0.16	0.41
A8–T19	-0.34	0.14	-0.37
C9–G18	-0.01	0.02	0.11
G10–C17	-0.05	-0.00	0.26
T11–A16	-0.01	-0.00	0.28
C12–G15	-0.00	-0.01	0.23
G13–C14	0.01	-0.00	0.01

Table S22: *Differences in rotational base pair parameters for 13merTAL and 13merRef*

base pair	Buckle (χ)/Â°	Propeller Twist (ω)/Â°	Opening (σ)/Â°
G1–C26	-0.1	0.1	-0.1
C2–G25	0.9	1.9	-0.3
T3–A24	4.8	-0.4	-0.2
G4–C23	3.9	-1.5	-0.1
C5–G22	-4.9	6.8	-0.6
A6–T21	-5.1	-7.8	-0.4
A7–T20	2.1	20.5	-4.3
A8–T19	11.4	22.5	5.0
C9–G18	-8.4	15.0	0.7
G10–C17	4.1	-9.3	0.2
T11–A16	-1.3	-13.7	1.0
C12–G15	-5.6	-5.1	0.5
G13–C14	-2.0	1.1	-0.1

Table S23: *Differences in translational base pair step parameters for 13merTAL and 13merRef*

base pair step	Shift (Sx)/Å	Slide (Sy)/Å	Rise (Sz)/Å
G1–C2	-0.02	0.18	-0.09
C2–T3	0.08	-0.10	-0.12
T3–G4	0.05	-0.21	0.14
G4–C5	-0.31	-0.11	0.25
C5–A6	0.36	-0.33	0.18
A6–A7	0.28	-0.67	-0.21
A7–A8	1.41	-0.58	0.10
A8–C9	-0.95	-0.60	0.86
C9–G10	-0.52	-0.16	-0.43
G10–T11	-0.00	-0.00	-0.01
T11–C12	0.01	-0.20	0.04
C12–G13	-0.00	-0.01	-0.10

Table S24: *Differences in rotational base pair step parameters for 13merTAL and 13merRef*

base pair step	**Tilt** (τ)/**Â°**	**Roll** (ρ)/**Â°**	**Twist** (Ω)/**Â°**
G1–C2	-0.8	3.9	0.6
C2–T3	-1.3	-3.5	-0.3
T3–G4	3.8	-3.2	-1.1
G4–C5	-4.1	7.0	0.2
C5–A6	-4.8	-8.0	-2.4
A6–A7	1.3	-2.0	-1.8
A7–A8	3.4	4.0	-7.8
A8–C9	-2.3	1.7	-3.4
C9–G10	1.9	-1.6	-2.9
G10–T11	-0.5	-1.2	1.8
T11–C12	-1.1	-3.3	0.8
C12–G13	1.6	-1.5	-0.5

7 Base pair lifetime measurements and Saturation transfer experiments

Exchange rates of the imino protons were obtained from inversion recovery experiments at 298 K. For this purpose the standard 1D 1H-WATERGATE pulse program was modified to start with a selective rectangle inversion pulse, centered on the imino proton region, of 327 μs duration. After a variable delay (21 settings) a 1D spectrum was recorded. Samples were prepared in H_2O with the buffer described earlier, and each duplex was titrated with 1 M TRIS buffer as base catalyst for proton exchange. At every titration point the pH was adjusted to $\approx$7.1 and the spectroscopic procedure was carried out three times, resulting in 693 1D spectra. Each spectrum was fitted by Lorentzians, and thereby the integral of the imino proton peaks was determined. An exponential fit of the signal integral vs delay time yields the spin-lattice relaxation time T_1.

Base pair lifetimes are extracted from the linear fit by extrapolation to infinite base concentrations. While they give information on the rate of the opening reaction, the apparent dissociation constant K_D which can be obtained from the slope of the fit gives access to the closing rates according to Eq. S1.

$$K_D = \alpha k_{iso} K_{diss} = \alpha k_{iso} \frac{k_{op}}{k_{cl}} \tag{S1}$$

α measures the accessibility of the exchanging imino site, k_{iso} is the exchange rate constant of the isolated nucleoside and $K_{diss}=k_{op}/k_{cl}$ is the equilibrium constant for dissociation reaction of the pertinent base pair. α and k_{iso} are assumed to stay unchanged upon introduction of the triazole moiety since the nucleoside itself is not altered chemically. The Gibbs energy for dissociating the base pair, $\Delta_{diss}G$, is changed when the phosphate backbone is replaced with the triazole linker, by

$$\Delta\Delta_{diss}G = -RT \ln \frac{K_{diss}^{TAL}}{K_{diss}^{Ref}} = -RT \ln \frac{K_D^{TAL}}{K_D^{Ref}} \tag{S2}$$

In Fig. S14 and S15 the linear fits for the plots of imino proton exchange times vs inverse base catalyst concentration are shown, together with the resulting basepair lifetimes τ_{op} and inverse apparent dissociation constants $1/K_D$.

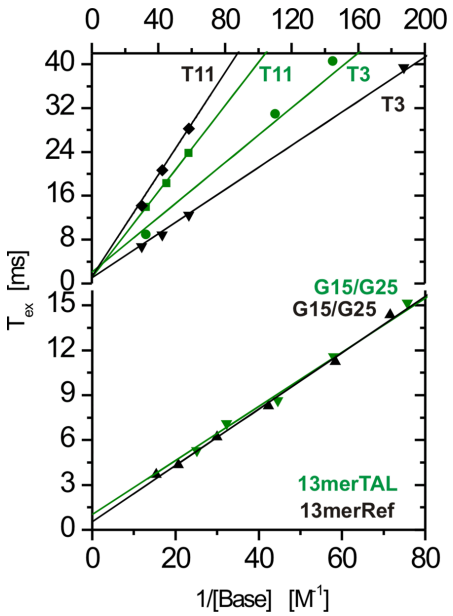

Fig. S14: *Linear fits for the imino proton exchange times of T3,T11,G15,G25 vs the inverse base catalyst concentration.*

The structural results of the main paper are also corroborated by saturation transfer experiments, which are indicative of the dynamics in the absence of added base catalyst. [S10] The reduction in signal for T19 and T20 imino protons is much more severe than for T3 although their τ_{op} is comparable (Fig. S16).

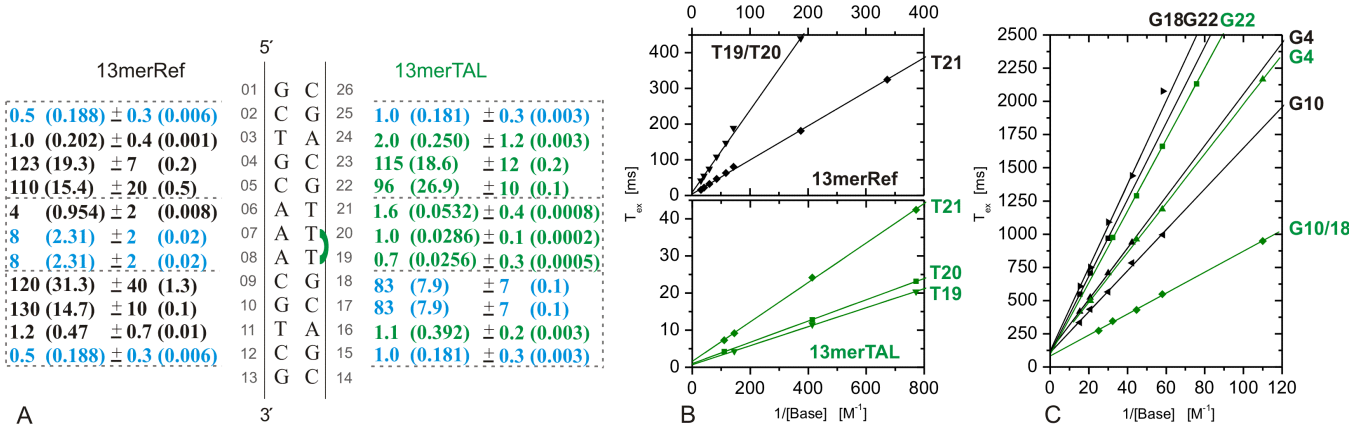

Fig. S15: *The basepair lifetimes τ_{op} (inverse apparent dissociation constants ($1/K_D$)) and their respective errors are tabulated in the left panel. They are determined by measuring the dependency of T_1 relaxation rates of imino proton signals on the concentration of TRIS base, which catalyzes exchange with water [S10] (middle and right panel). Values in blue could not be determined separately, but they should be similar because of identical recovery behaviour.*

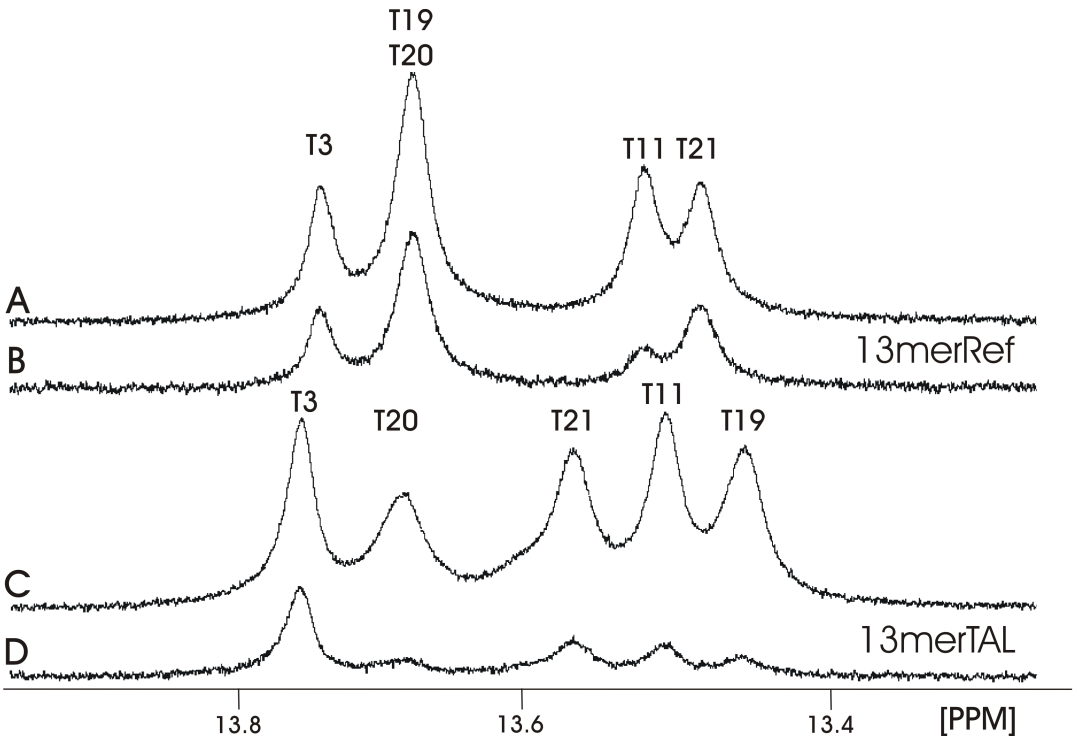

Fig. S16: *Saturation transfer experiments in H_2O at 298 K for 13merTAL (upper part) and 13merRef (lower part). [S10] Use of a strong saturation pulse for experiments B and D results in reduced signal intensities due to chemical exchange of the saturated protons of H_2O and the unsaturated imino protons. In experiments A and C the saturation of the water signal is largely avoided as the WATERGATE sequence is employed.*

References

(S1) G C K Roberts, editor. *NMR of Macromolecules: A Practical Approach*. Oxford University Press, 1993.

(S2) Victor A Bloomfield, Donald M Crothers, and Jr. Ignacio Tinoco. *Nucleic Acids: structures, properties and functions*. University Science Books, 2000.

(S3) Rochus Keller. *The Computer Aided Resonance Assignment Tutorial*. CANTINA Verlag, 1st edition, 2004.

(S4) Charles D Schwieters, John J Kuszewski, Nico Tjandra, and G Marius Clore. The Xplor-NIH NMR molecular structure determination package. *Journal of Magnetic Resonance*, 160:65–73, 2003.

(S5) Curt M Breneman and Kenneth B Wiberg. Determining atom-centered monopoles from molecular electrostatic potentials. The need for high sampling density in formamide conformational analysis. *Journal of Computational Chemistry*, 11(3):361–373, 1990.

(S6) Annaleen Vermeulen, Hongjun Zhou, and Arthur Pardi. Determining DNA Global Structure and DNA Bending by Application of NMR Residual Dipolar Couplings. *Journal of the American Chemical Society*, 122(40):9638–9647, 2000.

(S7) Olivier Mauffret, Georges Tevanian, and Serge Fermandjian. Residual dipolar coupling constants and structure determination of large DNA duplexes. *Journal of biomolecular NMR*, 24(4):317–28, December 2002.

(S8) Marcel Ottiger and Ad Bax. How Tetrahedral Are Methyl Groups in Proteins? A Liquid Crystal NMR Study. *Journal of the American Chemical Society*, 121(19):4690–4695, May 1999.

(S9) Jean-Luc Pons, ThïżœrïżœseE. Malliavin, and MarcA. Delsuc. Gifa V. 4: A complete package for NMR data set processing. *Journal of Biomolecular NMR*, 8(4):445–452, December 1996.

(S10) André Dallmann, Lars Dehmel, Torben Peters, Clemens Mügge, Christian Griesinger, Jennifer Tuma, and Nikolaus P Ernsting. 2-Aminopurine Incorporation Perturbs the Dynamics and Structure of DNA. *Angewandte Chemie (International ed. in English)*, pages 5989 –5992, July 2010.